EMITTER International Journal of Engineering Technology
Vol. 12, No. 1, June 2024, pp. 1~21
DOI : 10.24003/emitter.v12i1.839

Performance Evaluation of mm-Wave Based System in GFDM-5G and Beyond Channel Model with Dust Storm Scenario

Zainab Sh. Hammed[1,2], Siddeeq Y. Ameen[1]

[1] Department of Energy Engineering, Technical College of Engineering, Duhok Polytechnic University, Duhok, Kurdistan Region, Iraq
[2] Department of Electrical and Computer, College of Engineering, University of Duhok, Kurdistan Region, Iraq
Corresponding author: zainab.shawqi@dpu.edu.krd

Received September 9, 2023; Revised October 22, 2023; Accepted February 16, 2024

Abstract

Telecommunication has made tremendous improvements in terms of bandwidth, requiring good frequency location, high data rates, and wideband spectrum availability. One solution to these requirements is the millimeter wave frequency band of 30 GHz. However, communication in this band is facing new challenges due to climate effects such as humidity, dust storms, and temperature. For fifth-generation (5G) mobile networks and beyond, Generalized Frequency Division Multiplexing (GFDM) has been proposed as a compelling candidate to substitute Orthogonal Frequency Division Multiplexing (OFDM). The GFDM's ability to adapt the block size and type of pulse shaping filters enables it to meet various crucial requirements, including low latency, low Out-Of-Band(OOB) radiation, and high data rates. This paper evaluated the overall GFDM performance and investigated the Bit Error Rate (BER) across a Rayleigh channel under various weather conditions. The simulation results show that GFDM outperforms the current OFDM candidate system. Also, GFDM offers better resistance to the Rayleigh channel with moderate and heavy dust storms in terms of BER.

Keywords: Pulse-shaping filter, GFDM, OFDM, Physical-Layer, OOB radiation.

1. INTRODUCTION

The fifth-generation (5G) and beyond wireless system will improve on the capabilities of the fourth-generation (4G) standards to serve more users and provide high data rate communication. To that end, 5G system carriers will be able to operate at higher frequency bands, such as millimeter-wave (mm-wave) bands spanning 30 GHz to 300 GHz, to achieve greater bandwidths and higher data rates[1][2]. Currently, OFDM has been the standard candidate waveform in the 5G mobile communication system primarily due to its ease of implementation using the algorithms of the Fast Fourier Transform (FFT) [3].

5G network application scenarios face issues that OFDM can only handle to a certain extent. For example, Machine-to-Machine (M2M) and Machine-Type Communication (MTC) need minimal power consumption, making the stringent synchronization procedure necessary to maintain subcarrier orthogonality costly [2] [3]. Low latency time needed for Tactile Internet (TI) applications necessitates tiny bursts of data, indicating that signals using OFDM, each of which had just a single Cyclic Prefix (CP), would have extremely low spectral efficiency [4]. Therefore, more flexible multicarrier modulation techniques have been suggested for next-generation communication, such as Filter Bank Multicarrier (FBMC) [5], which uses pulse-shaped subcarriers to decrease OOB emissions. The drawback of FBMC, it's not appropriate for low-latency cases when high efficiency requires rapid burst transmissions [5].

UFMC (Universal Filtered Multicarrier) is another approach for reducing OOB emissions by filtering a collection of subcarriers [6]. UFMC is more susceptible to slight distortion than Cyclic Prefix–Orthogonal Frequency Division Multiplexing (CP-OFDM). The weak point of UFMC may not be convenient for energy-saving applications that need loose time synchronization [7]. Thus, another technique known as GFDM has been suggested (8). GFDM is a block-based modulation technique, where each block contains several sub-carriers and sub-symbols. A prototype filter that is circularly shifting in frequency and time domain filters subcarriers [8]. As a result, Out-Of-Band (OOB) emissions are reduced, allowing for both dynamic spectrum and fragmented spectrum allocation without causing significant disturbance to incumbent users or services [9]. The GFDM block's overhead is kept as low as possible by using a single CP for the whole block, which enhances the system's spectral efficiency. In addition, all of the primary synchronization algorithms established for OFDM may modify GFDM [9].

The increasing duststorms and sand that had lately occurred in nations of the Middle-East as a result of global warming and deployment of 5G and beyond in wireless and mobile communication systems are the primary drivers behind the need to conduct such an inquiry. Thus, in this paper, the performance of GFDM needs to be studied more closely with the effects of weather climates such as the dust storm, which become more common in arid regions of the world, especially nations in the Middle East such as Iraq and Kuwait, as well as those in the Arab Gulf. This will identify the objectives of this paper is to assess effectiveness of mm-wave based systems in GFDM for 5G and beyond in terms of dust rate influence in a wider range of dust criteria, particularly very heavy, moderate, and no dust. As a result, we conducted research on the impact of dust rate on 5G performance analysis by examining the BER and outage effectiveness of various modulation waveform techniques, including OFDM and GFDM, in mm-wave-based systems. Furthermore, the GFDM system is thoroughly investigated to determine the impact of parameters on system's Out-Of-Band (OOB) emission.

The paper is organized as follows : Section II describes the related work. Section III, a short description of the GFDM system, is represented in the notation used throughout this study. Section IV contains the system performance. Finally, Section V discusses the conclusions.

2. RELATED WORKS

GFDM is a modulation and multiple access scheme that has been proposed as a potential candidate for the physical layer of 5G and beyond wireless communication systems. It is designed to overcome some of the limitations of traditional OFDM and enable efficient spectrum usage, improved flexibility, and better coexistence with other wireless technologies [10]. Several research works and studies have been conducted on GFDM in the context of 5G. Here are some notable related works:

A comparison between GFDM and OFDM to evaluate the latency and throughput performance of both techniques is presented in [11]. In [12], GFDM with filtering techniques and clipping was proposed, and its performance in terms of peak to average power ratio (PAPR) was presented. According to the simulation results, at equal spectral efficiency (ESE), the PAPR of clipped and filtered GFDM signals is reduced by 1.6 dB when compared to clipped and filtered OFDM signals with nearly similar BER performance. Furthermore, for equal spectral efficiency conditions, the complexity of the GFDM system is less than that of the OFDM system. In [13], authors compared a number of 5G waveform candidates (UFMC, GFDM, OFDM, and FBMC) within a shared framework. They assessed power spectral density, spectral efficiency, peak-to-average power ratio, and robustness to asynchronous multiuser uplink transmission. Moreover, they evaluate and compare the various waveforms's complexity.

The performance of the offset QAM-based GFDM is considered in [14], in addition to the analysis of symbol error performance under various fading conditions. Outdoor fading profiles such as Urban Approaching Line of Sight (UALOS),Highway Line of Sight (HLOS), and Rural Line of Sight (RLOS) are used to assess GFDM-OQAM system effectiveness.

Many studies used New York University Wireless Simulator (NYUSIM) to generate spatial channel responses for 5G communication and to investigate MIMO system performance at 28 and 73 GHz [15][16][17]. E. D. Wardihani et al. [18] used NYUSIM to study the channel model for Semarang city under three rainfall conditions and provide additional information about water evaporation as an atmospheric pressure attenuation.

In [19], NYUSIM is used to investigate the effect of a dust storm on 5G at 28 GHz and 70 GHz. For simulation Massive MIMO of 128 x 128 with equally spaced URA was investigated and the BER and outage performance were examined for GFDM at different dust storm criteria, i.e., very heavy, moderate, and clear weather, and compared with OFDM at the same standards.

Previous research focused on the impact of sand and duststorms on a single transmitter and receiver (T_X/R_X) antenna using the orthogonal frequency division multiplexing (OFDM) technique. As a result, the primary contribution of this research is to investigate effects of duststorms and sand on millimeter-wave frequencies in the context of the generalized frequency division multiplexing (GFDM) technique, which is applicable to 5G and future generations of wireless communication. This research uses real data from sand and dust storms in an urban environment. The reason for this research is especially important given the recent increase in dust and sand storms in Middle Eastern countries caused by climate change, in addition to the deployment of 5G and beyond technologies.

3. ORIGINALITY

The important motivating factor for such investigation is very crucial because of the increased duststorms and sand recently in the Middle East countries because of climate change and the adoption of 5G and beyond. Real data from a dust and sand storm in an urban setting is used in this investigation. A previously conducted study used the OFDM in 5G to investigate the effects of a sand and dust storm on a single T_X/R_X antenna.

As an extension to the previous study and finding a better system, a GFDM system has been investigated to evaluate the performance of the GFDM in 5G and beyond with dust storm scenario. This investigation will be the main contribution of the study and originality. Moreover, the results of the GFDM is compared with those of orthogonal frequency division multiplexing (OFDM), the conventional waveform for 4G and 5G networks. The outcome demonstrates that, in terms of bit error rate (BER), GFDM performs better than OFDM in the presence of dust and sandstorm with the 5G and beyond parameters.

4. SYSTEM DESIGN

The fundamental hypothesis of the GFDM systems is that it is impossible to achieve 5G requirements by keeping rigid standards on orthogonality and synchronization. In the GFDM scheme, orthogonality between the subcarriers is abandoned as they are separately filtered through a so-called "prototype" pulse shape filter [8] [20]. The data is divided into blocks that span the transmitted signal onto K subcarriers and M time slots, during which symbols are sampled N times. Then a single CP is added to this block [9], as shown in Figure 1.

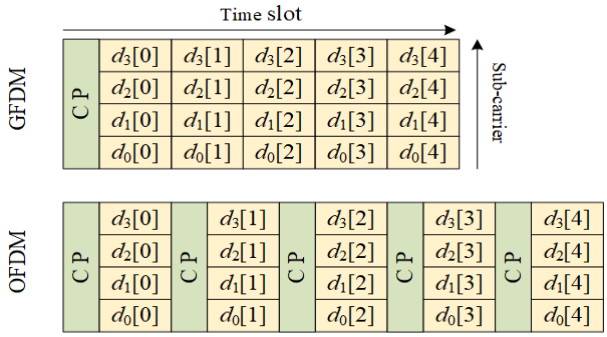

Figure 1. GFDM vs OFDM block structure

4.1. Transmitter Model

The baseband GFDM transmitter's block diagram is depicted in figure 2.

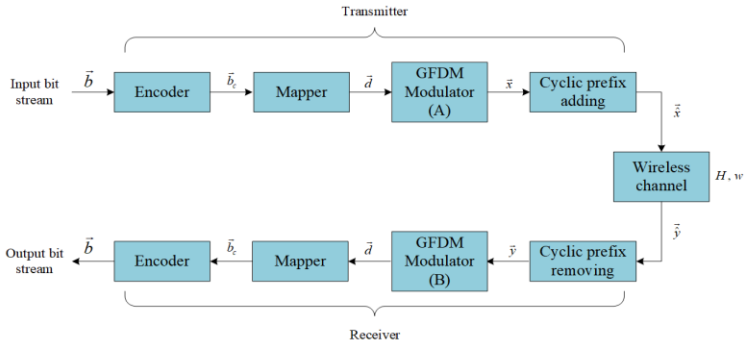

Figure 2. Transceiver block diagram

In the block diagram, a binary data vector $\vec{b}$ is provided by a data source, which is encoded to obtain $\vec{b}_c$. $\vec{b}_c$ is mapped to symbols $\vec{d}$ by a mapper, for instance, Quadrature Amplitude Modulation (QAM) and Phase shift keying (PSK) [21]. Thus, a vector $\vec{d}$ is the data block that contains a total of KM elements, which will then get divided into K sub-carriers with M sub-symbols, as shown in Figure 3. This reshapes the vector $\vec{d}$ into $(d_0^T, d_1^T, \ldots\ldots, d_{M-1}^T)^T$, where $d_m = \left(d_{0,m}, d_{1,m}, \ldots, d_{K-1,m}\right)^T$.

$$\overline{d} = \begin{pmatrix} d_{0,m} \\ d_{1,m} \\ \vdots \\ d_{K-1,m} \end{pmatrix} \begin{pmatrix} d_{0,0}\, d_{0,1} \ldots d_{0,M-1} \\ d_{1,0}\, d_{1,1} \ldots d_{1,M-1} \\ \vdots \quad \vdots \quad \ldots \quad \vdots \\ \vdots \quad \vdots \quad \ldots \quad \vdots \\ d_{K-1,0}\, d_{K-1,1} \ldots d_{K-1,M-1} \end{pmatrix} \tag{1}$$

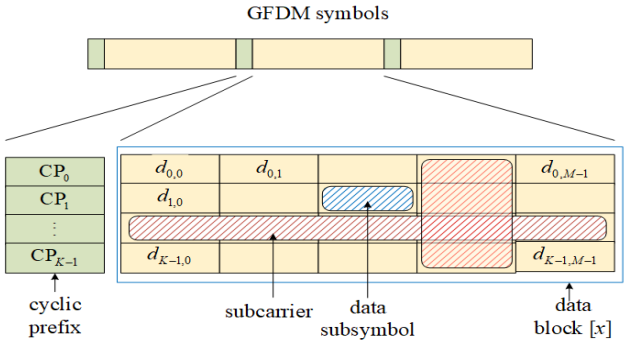

Figure 3. Overview of GFDM block structure and terminology

Each $d_{k,m}$ element corresponds to the data transmitted on the Kth sub-carrier, and, in a m_{th} time slot, the vector $\vec{d}$ is then passed to the GFDM modulator [22]. The structure of the GFDM modulator is shown in Figure 4. A factor upsamples the complex data symbols, i.e. L-1 zero is appended to ensure aliasing.

$$d_k[n]=\sum_{m=0}^{M-1} d_k[m]\delta[n-mL],n=0,...,N-1 \quad (2)$$

where δ[.] is the Dirac function. Consequently,d_k [n=mL] = d_k[n] and d_k [n=mL]

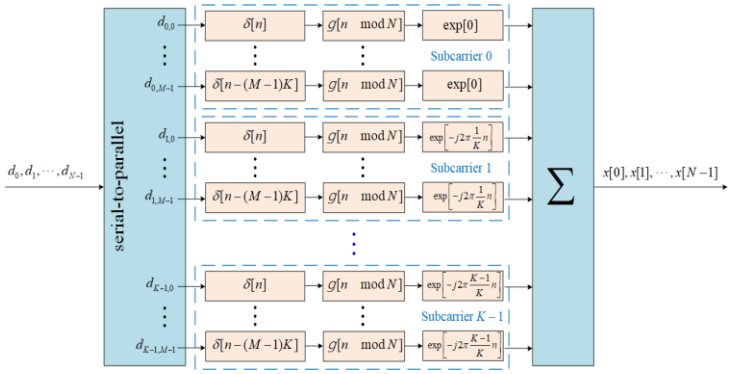

Figure 4. Details of the GFDM modulator

Each upsampled sub-carrier are filtered individually with a corresponding pulse shape filter $g_{k,m}[n]$,

$$g_{k,m}[n] = g[(n-mK) \bmod N].\exp\left[-j2\pi\frac{k}{K}n\right] \quad (3)$$

where $g_{k,m}[n]$ is a frequency and time-shift variant of a prototype filter $g[n]$, in which at each sub-carrier a copy is delayed by mK in time and shifted by $\frac{k}{K}$ in the frequency domain, where $\frac{1}{K}$ denotes the subcarrier spacing. The filter is circular with periodicity n-mK to facilitate tail biting, preventing the up and down ramps of the signal, which generally limit the efficiency of

transmissions [23]. Figure 5 shows some different types of pulse shape-filters that have been utilized in GFDM.

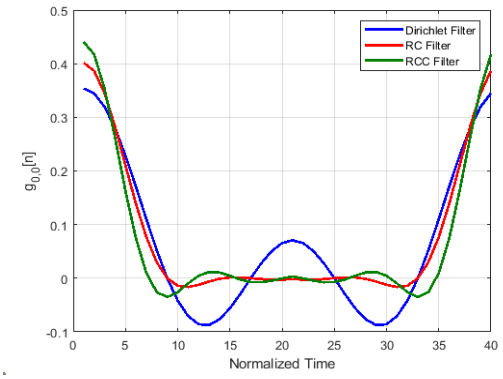

Figure 5. Time- domain responses of different pulse shaping filters used in GFDM.

Finally, the baseband transmitted signal $\vec{x}=(x[n])^T$ in the digital domain is produced by superimposing all subcarrier symbols.

$$x[n]=\sum_{k=0}^{K-1}\sum_{m=0}^{M-1} g_{k,m}[n]d_{k,m} \quad (4)$$

The above model can also be formulated as a multiplication of two matrices [24].

$$\vec{x} = A\vec{d} \quad (5)$$

where A is a KM × KM modulation matrix with a structure as

$$A = \left(\vec{g}_{0,0}\cdots\vec{g}_{K-1,0}\vec{g}_{0,1}\cdots\vec{g}_{K-1,1}\cdots\vec{g}_{K-1,M-1}\right) \quad (6)$$

In the modulation matrix A, the absolute value is shown in Figure 6. The matrix includes the responses of the pulse shaping filter for all possible subcarriers. Finally, a CP is added to $\vec{x}$ to obtain the signal $\vec{\tilde{x}}$ that is transmitted over a wireless channel [25].

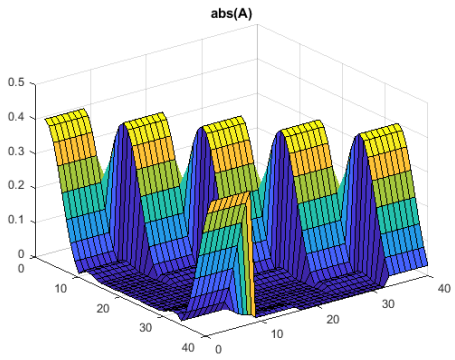

Figure 6. The Transmitter A matrix for N=56, K=8 and M=5 with RC filter and roll-off factor a=0.5.

4.2 Receiver Model

After the modulated signal passed through a wireless channel system, assuming perfect synchronization, a received baseband sampled was obtained according to

$$\vec{y} = H\vec{x} + \vec{w} \quad (7)$$

where $\vec{y}$ is a vector containing the unequalized time samples at the receiver. H is the channel convolution matrix constructed from a channel impulse response, and $\vec{w}$ is the additive white Gaussian noise (AWGN) [24] [26]. A general transceiver equation can be expressed as:

$$\vec{y} = HA\vec{d} + \vec{w} \quad (8)$$

Introducing $\vec{z} = H^{-1}HA\vec{d} + H^{-1}\vec{w}$ as the received signal after channel equalization, linear demodulation of the signal can be expressed as

$$\hat{\vec{d}} = B\vec{z} \quad (9)$$

where B is a $KM \times KM$ receiver matrix according to the transmitter's and receiver's specifications.

GFDM is classified as a filtered multicarrier system (FMS). The term is derived based on the scheme providing more variance than ordinary OFDM; when M = 1, GFDM becomes OFDM. The fundamental characteristic that separates GFDM from OFDM and Single-Carrier Frequency Domain Equalization (SC-FDE) is that, like Single-carrier frequency-division multiple access (SC-FDM), it allows for the subdivision of a particular time-frequency resource into sub-symbols and sub-carriers of M and K. As a result, the spectrum can be designed to meet specific needs, and pulse shaping is conceivable on the basis of per-subcarrier. As a result, the sampling frequency has not been modified.

The mm-Wave MIMO system shown in Figure 7 is a combination of two consecutive joint segments: an analog RF precoder and a digital MIMO baseband. This system has radio frequency (RF) chains, NS parallel data streams, N_T transmitters at the base station (BS) and N_R receivers at the mobile station (MS), and $N_{RF} \leq \min(N_T, N_R)$ at the transmitter and receiver. At the transmitter, N_{RF} chains are present, such that $N_S < N_{RF} < N_T$.

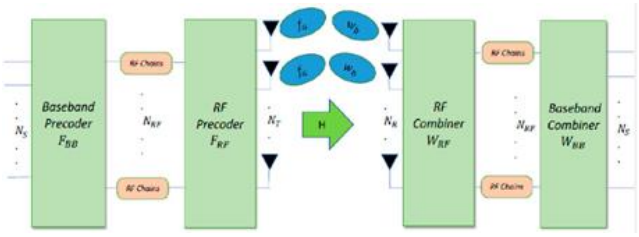

Figure 7. Block diagram of a mmWave massive MIMO system

The GFDM has been designed to use a significant number of narrowband subcarriers to occupy a part of the bandwidth, as opposed to a

limited number of subcarriers with very high individual bandwidth, as in Single-carrier FDMA (SC-FDM) or OFDM. Moreover, it's interesting with the addition filtration systems, GFDM remains a block-based technique. User scheduling in a multi-access environment should consider these aspects while aiming for low-latency transmissions. As well as in the case of high-speed data transfers [27].

4.3 Characterization of Dusty channels

The transceiver block diagram illustrated in Figure 2 is considered the system model in this paper. A bandwidth of 800 MHz has been selected at an operating frequency of 28 GHz, which is employed for 5G and beyond. In this system, H represents the channel's attenuation coefficient, including dust effects, and is a random variable that is dependent on characteristics of the dust to evaluate GFMD's performance in terms of BER.

On Earth, dry and semi-arid regions are frequently home to dust and sandstorms. These conditions appear when the wind lifts ground-bound dust particles into the air. These storms are typically witnessed throughout the year in various Middle Eastern locations, particularly in Iraq, Kuwait, and Saudi Arabia.

Generally, dust storms typically occur over arable land where there has been a prolonged drought. Depending on the location, strong winds can propel dust particles up to a few kilometers in height. Particle dust diameters range from 100 m to 1 m, with sand particles typically measuring 0.15–0.3 mm. As a result, the fall speeds of such particles are such that the dust may reduce visibility for extended periods. The visibility must be less than 1 km to be classified as a dust storm. A severe dust storm occurs when visibility is less than 500 meters [28]. Thus, the attenuation distribution varies significantly across the channel due to the variation in sand and dust diameters. Moreover, at mm-wave frequencies, with increasing atmospheric effects and environmental factors such as dust storms, rain rate, temperature, humidity, and air pressure, the attenuation loss would significantly impact [29]. However, attenuation loss affected by distance; because mm-wave frequencies only cover a small area (less than 1 km), attenuation is minimal when compared to UHF frequencies [30] [31]. Particular attenuation measured in dB/km, if the radius cell on 5G technology is just 200 m, the radius cell will be lowered by approximately 80% and may be adjusted by employing high gain on steerable antennas[32] [33].

4.4 Path Loss Model

Path loss, typically measured in decibels (dB), describes the power loss in signal power relative to transmit power P_{TX}, which is affected by link distance d and carrier frequency fc. The close-in (CI) free-space path loss (FSPL) model is a straightforward path loss model that is described as [30]. At a reference distance of 1 m, the following equation accounts for atmospheric attenuation and free space path loss [34]:

$$PL^{CL}(f,d)[dB] = FSPL(f,1m)[dB] + 10n\log_{10}(d) + AT[dB] + X_{\sigma}^{CL} \quad (10)$$

where $d \geq 1m$, f is the carrier frequency (GHz), d is the distance, AT is the attenuation term, PL^{CL} a path loss exponent, and (X_{σ}^{CL})Gaussian random variable with a standard deviation. The path loss between the transmitter and receiver (T-R) at a distance of 1 m, expressed in dB, is known as the free space path loss (f, 1m) and given by:

$$\begin{aligned} FSPL(f,1m)[dB] &= 20\log_{10}\left(\frac{4\pi f\times 10^{9}}{c}\right) \\ &= 32.4[dB] + 20\log_{10}(f) \end{aligned} \quad (11)$$

where c is light's speed in a vacuum is equal 299792458 m/s ≅ 3 × 10^8 m/s, and f is the frequency in GHz. AT is differentiated by the following features:

$$AT[dB] = \alpha[dB/m]\times d[m] \quad (12)$$

where α in dB/m is the attenuation factor between 1 GHz and 100 GHz. This factor considers water vapor's impacts, haze, rain, and arid atmosphere attenuation [34]. In addition to the FSPL, atmospheric absorption affects radio signals traveling through open space. Once more, both frequency and distance affect the attenuation caused by air absorption [35] [36].

4.5 Delay Spread and Power Delay Profile:

When receiving a signal in a multipath environment, power-delay -profile (PDP) a critical evaluating signal intensity. Several aspects of multipath channel time dispersion can be characterized using delay spread. It has been thought to form from PDP, and because it is a group of highly energetic multipaths, it may be disseminated across the latter. Additionally, the channel downlink signal is an essential statistic for calculating the amount of system overhead required for optimal communication. The root means square approach can be used to calculate delay spread, with the starting point being the power delay profile's second central instant. The following may be used to calculate the delay spread [15]:

$$\sigma_t = \sqrt{\overline{t^2} - (\bar{t})^2} \quad (13)$$

where

$$\overline{t^2} = \frac{\sum_n p(t)t_n^2}{\sum_n p(t_n)} \;\&\; \bar{t} = \frac{\sum_n p(t)\tau_n}{\sum_n p(\tau_n)} \quad (14)$$

where $\bar{t}$ is the parameter that has an excess mean delay; it is the first central moment. $\overline{t^2}$ is the second central instant of power delay profile, and the milliwatt power of the corresponding delay to the delay bin t_n is $p(t_n)$.

4.6 Channel links budget:

The SNR in wireless systems computed using data from radio links and described as [37]:

$$SNR=P_t + G_t + G_r - \overline{PL} - N_o - IL \quad (15)$$

where G_t and G_r are the antenna gains of T_X and R_X, which in this test are both 3 dB, and Pt is the transmitting power. In the measurements, IL stands for the expected 6 dB total implementation loss. N_0 total noise power, is computed as follows:

$$N_0 = 10\log_{10}(kTB) + NF \quad (16)$$

where k is the Boltzmann's constant, the room temperature is T= 290 K, and NF is the noise figure at R_X, 6 dB expected. It should be noted that the IL and NF are set to the identical values as those in [37].

In measurement environments, the mean path loss, denoted by PL is represented mathematically as:

$$\overline{PL}_{LOS}(d) = + 61.1419.8 \log(d) \quad (17)$$

and

$$\overline{PL}_{NLOS}(d) = + 61.440.6 \log(d) \quad (18)$$

for the LOS and NLOS channels, respectively.

5. EXPERIMENT AND ANALYSIS

The system performance was conducted by a channel modelling and simulation using the New York University Wireless Simulator (NYUSIM) and MATLAB to examine the GFDM performance. The NYUSIM, simulator is developed by NYU Wireless, uses the numerology of 5G [38] [39]. This simulator can be used to generate realistic temporal and spatial channel responses to support realistic physical- and link-layer simulations, as well as the 5G cellular communications system [15].

Analytical expressions is obtained to analyze the system's BER performance, taking into consideration what is discussed in Section II. In GFDM-based systems, the overall bit error probability is given by

$$P(e)= \frac{1}{N} \sum_{n=0}^{N-1} P_n(e) \quad (19)$$

where $P_n(e)$ denotes the bit error probability of the nth sub-carrier, and N is the total number of sub-carriers. The decision variable (d_k) with h = H can be defined as follows to acquire this error probability:

$$d_k = \frac{yk}{H} = x_k + \frac{z}{H} \quad (20)$$

It should be noted that the decision variable can be thought of as a symbol x_k distorted by zero mean and zero variance Gaussian noise $N_0/|H|^2$. As a result, the nth subcarrier's bit error probability can be calculated by

$$P_n(e)= \int_{-\infty}^{\infty} P_n(e|h=H)_{ph}(H)dH \quad (21)$$

The right side's conditional probability of equation (20) depends on the modulation technique employed in the n-th subcarrier [40]. It is feasible to discover estimated formulas in the literature for the main digital modulations, such as MPSK and MQAM, by using

$$P_n(e|h=H) \approx \frac{2}{\log_2 M} Q\left(\sqrt{|H|^2 \gamma_b} \log_2 M \sin\left(\frac{\pi}{M}\right) \right) \quad (22)$$

and

$$P_n(e|h=H) \approx \frac{2}{\log_2 M} Q\left(\frac{\sqrt{3|H|^2 \gamma_b \log_2 M}}{M-1} \right) \quad (23)$$

respectively. In each of these formulations, γ_b indicates the signal-to-noise ratio per bit, which can be written $\gamma_b = E_b/N_o$. The configuration parameters for the GFDM and OFDM are shown in Table 1. To ensure a fair comparison, both systems are designed with similar parameters. Tables 2 and 3 list the channel and antenna parameters, respectively.

Table 1. Simulation parameter For GFDM System

Parameter	Description	Realistic Values
K	Samples presub-symbol	128
M	sub-symbols	7,9 for GFDM, 1 for OFDM
CP	Cyclic Prefix	0.1
Pulse	Pulse- shaping- filter	RRC: Root-Raised Cosine RC: Raised Cosine Dirichlet
∝	Roll-off factor of a pulse-shaping-filter	0.2, 0.9
mu	Modulation of QAM and PSK	4,8,16 for PSK, 16,32 for QAM
Subcarriers	Allocated sub-carrier	1: K
Sub symbols	Allocated sub-symbols	1: m for GFDM, 1 for OFDM
blocks	Number of blocks	10

Table 2. Input Channel Parameter

Antenna Parameters	values
No. of Tx antenna	1
No. of Rx antenna	1
Tx -antenna azimuth Half Power Beam Width (HPBW)	10^0
Tx -antenna elevation HPBW	10^0
Rx -antenna azimuth HPBW	10^0
Rx -antenna elevation HPBW	10^0
Tx- antenna Spacing Distance	0.5 λ
Rx –antenna Spacing distance	0.5 λ

In the simulation, channels were simulated with weather effects like dust storms, sand, humidity, temperature, and plants. The NYUSIM was used to simulate the channel model. Frequencies between 2 and 100 GHz were used in the simulation. Two scenarios of dust storms were considered in this study: the first is a moderate dust storm that arose when the humidity was 50% and the visible range was between 0.5 and 1 kilometer based on how far away the dust storm was from the observation location. The second scenario is severe dust with a humidity of 0% and a visible range of less than 0.5 kilometers.

Table 3. Antenna Parameters

Parameters	values
Frequency band	28 GHz
RF Bandwidth	800 MHz
System Scenario	Uma
Environment	LOS
Lower- Bound of T-R distance	10 m
Upper -Bound of T-R distance	100 m
Tx Power	30 dBm
BP (Barometric Pressure)	1013.25 mbar
Humidity	0, 50, and 100 %
Temperature	45 ◦ C
Rainfall Rate	0 mm/hr.
Polarizations	Co-Pol
Foliage rate	0.4 dB/m
Type of Array of Transmitters	Uniform Rectangular Array
Type of Array of Receiving	Uniform Rectangular Array

Figure 8 shows the power delay profile for two scenarios for clear and dusty weather. Consequently, one possible conclusion is that the signal attenuation rises with the dust storm's strength. Another apparent inference is that the attenuation of signals increases according to the frequency of incoming electromagnetic waves. In addition, the received power for the dust and clear effects dropped from -70.3 dBm to -79.7 dBm, respectively.

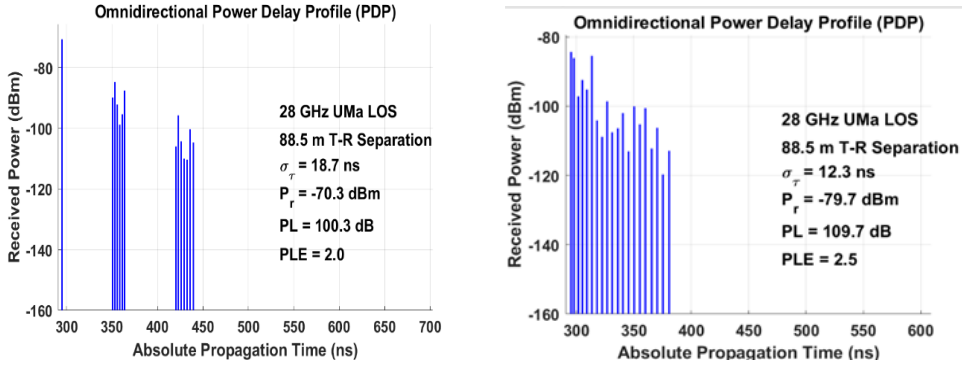

(a) (b)

Figure 8. Omnidirectional- PDP at 28,73 GHz. (a) clear weather. (b) with the effect of dust and sand

5.1 OOB Radiation

A comparison of power spectral density (PSD) for GFDM and conventional OFDM illustrated in figure 9. It can be shown that PSD curve of GFDM is better than OFDM because GFDM uses a prototype filters, and waveform shaping to reduce inter-carrier interference (ICI) and OOB of the signal. These characteristics make GFDM more spectrally efficient, interference mitigation and robust to frequency offsets than OFDM.

In addition; as the number of sub-symbols (M) in the GFDM rises, it can be shown that the OOB radiation of traditional GFDM is lower than that of OFDM. This can be considered a particular case of GFDM with M = 1 as the worst case. These benefits become even more pronounced as the number of subsymbols increases, making GFDM a promising candidate for future wireless systems that demands spectral efficiency, adaptability, and interference mitigation. In this article, it is assumed that M= 10.

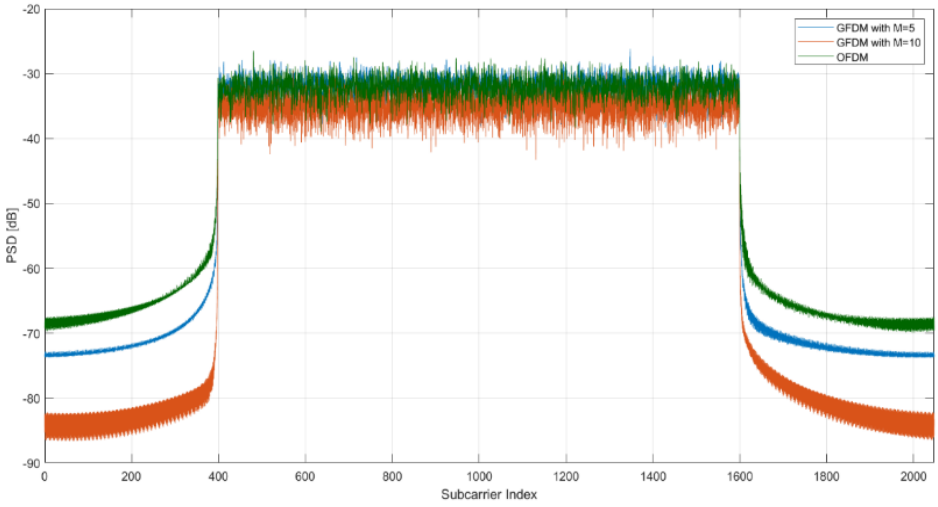

Figure 9. Power Spectral Density (PSD) of both GFDM and OFDM

5.2 BER performance

Figure 10 examines the quality of the GFDM with different modulation techniques. It can be shown that in terms of BER, 4PSK outperforms MQAM. 16QAM has a lower BER compared to 16PSK. The poor performance of MPSK compared to MQAM results from the arrangement of constellation points, where the possibility of one constellation point overlapping another when the signal picks up some noise is higher.

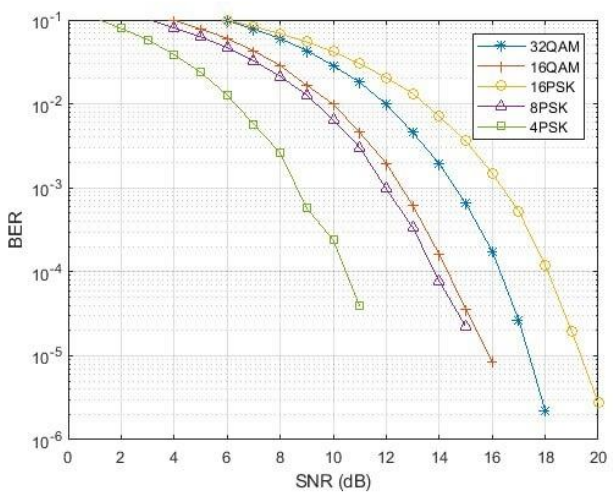

Figure 10. BER Comparison of the utilization of different modulation techniques with different modulation order in GFDM

The BER for both GFDM and OFDM in the Rayleigh channel with the dust condition is shown in Figure 11. A number of multipaths in a Rayleigh fading channel model of MIMO 5G and beyond is not a fixed or universal value, but it can range from 1 to 10 or more, depending on the channel conditions and the antenna configuration. For this article the number of multipath of dusty weather scenario is set to 10. The BER rate degraded heavily due to the dusty storm, with a slight advantage gained with the use of the GFDM over the OFDM. Furthermore, it can be noticed that the GFDM suffers a performance loss due to the dust storm but is still better than OFDM.

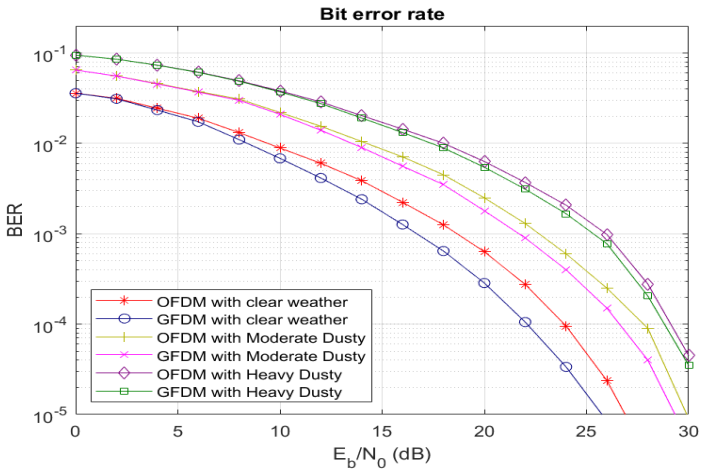

Figure 11. BER at f = 28 GHz of mm-wave systems over a dusty channel

5.3 Filter performance:

The GFDM uses pulse filters to shape the subcarrier pulses, they increase spectral efficiency and decrease signal peaks. Also; GFDM has a flexible structure that can adapt to different channel conditions and user

requirements. However, the GFDM is not immune to nonlinear distortion, as it still has some residual peaks and non-orthogonality in the frequency domain. Therefore, some techniques can be used to reduce the impact of nonlinear distortion on GFDM systems, such as pre-distortion, post-distortion, or equalization. Pre-distortion in the GFDM is a technique that applies an inverse function of the high power amplifier (HPA) nonlinearity to the input signal, so that the output signal is linearized and undistorted. Additionally; it could improve the performance of the GFDM systems in terms of BER, as shown in figure 12. GFDM with predistorter performed better than GFDM without predistorter. Additionally; spectral efficiency (SE), and PAPR by compensating the nonlinear distortion caused by the HPA. As illustrated in figure 13 for complementary cumulative distributive function (CCDF) curve, GFDM's PAPR decreased from 9.8 to 8.7 with a probability of 10^{-2} upon the OFDM's PAPR. The noticeable performance is excellent; it should be about 5 dB in order to be used in a setting with thousands of users.

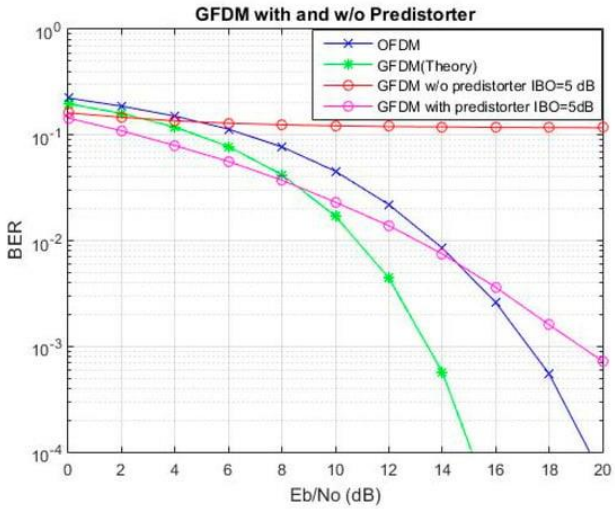

Figure 12. Comparing GFDM with and without a predistorter [41]

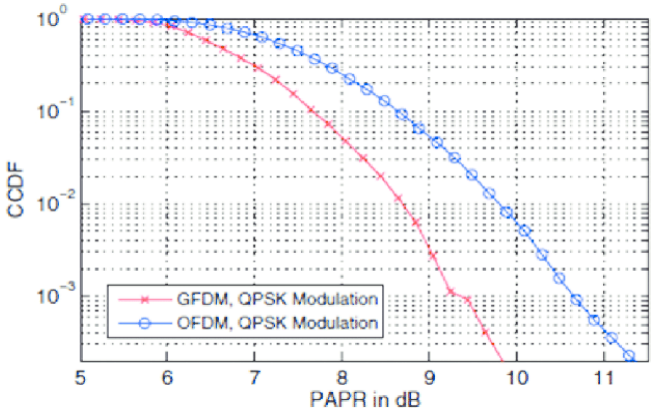

Figure 13. The PAPR of GFDM and OFDM with pre-distortion comparison [42]

Figure 14 exhibits the influence of the pulse-shaping filter on the BER performance of the GFDM. Three types of pulse filtering investigated (Raised Cosine RC, Raised Cosine and Root Raised Cosine RRc, and Dirichlet). It can be shown that Dirichlet filter has better performance than RC and RRC. The GFDM system is made orthogonal using the Dirichlet filter, which achieves the same BER as OFDM. Additionally, it has the ability to diminish OOB radiation. Moreover, roll-off factor value in RC and RRC have an effect on the BER. The roll-off value can decrease the BER distinctly.

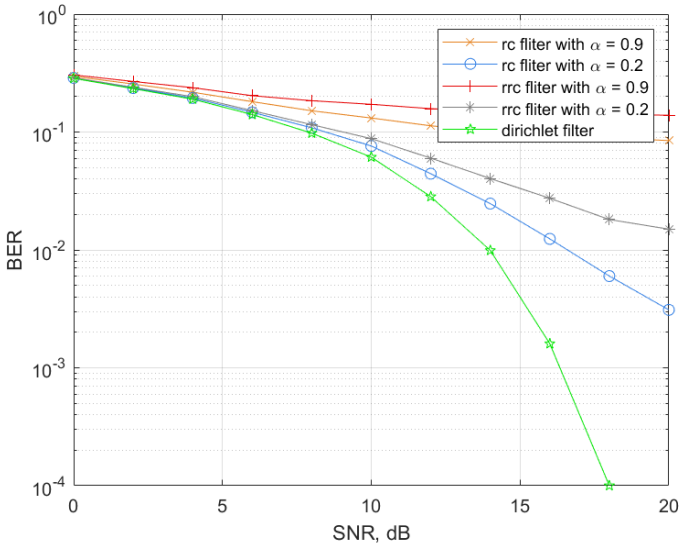

Figure 14. Impact of the pulse shape filter on BER in GFDM system

The simulation results also show that the performance of the GFDM in terms of BER with the Rayleigh channel outperforms that of the OFDM for the case of a heavy dust storm. However, the GFDM still has better spectrum properties than OFDM and lowers OOB emission by allowing some self-interference, an essential consideration in today's communication systems. The GFDM decreases the OOB radiation by 30% compared to that of the OFDM, according to simulation results. In previous study, the impact of dust storm and sand on a single Tx/Rx antenna using the OFDM technique was examined. Thus, a principal contribution of this article is to investigate how dust storms and sand impact on mm-wave in GFDM 5G and beyond. This investigation uses actual data from a sand and dust storm in an urban scenario.

6. CONCLUSIONS

Several challenges have arisen during the assessment of OFDM in mm-wave-based for 5G and beyond, particularly concerning the BER and OOB emissions characteristics in the presence of different levels of dust influence, ranging from heavy to moderate and no dust conditions. This research paper addresses these issues by proposing the use of GFDM as a potential solution

to mitigate OOB emissions and BER impact in OFDM, specifically when operating in diverse weather climates. The simulation results indicate that the GFDM stands out as the most promising modulation scheme for 5G and future networks, even when faced with the challenges posed by dust storms. Although the GFDM's performance is negatively affected by the presence of dust storms, it still outperforms OFDM in such scenarios. However, it is evident that dust storms have a substantial impact on system performance, leading to signal attenuation, increased path loss, and reduced link reliability. These adverse effects are primarily attributed to the scattering, absorption, and diffraction of mm-Wave signals by dust particles, resulting in signal degradation and potential data loss. The GFDM exhibits better spectral containment compared to OFDM, resulting in reduced interference with neighboring channels by 30 dB.

REFERENCES

[1] B. Alfaresi, Z. Nawawi, R. F. Malik, K. Anwar, and L. O. Nur, **Humidity Effect to 5G Performance under Palembang Channel Model at 28 GHz**, *Sinergi*, vol. 24, no. 1, pp. 49–56, 2020.

[2] Y. Zhou, Y. Zhang, M. Liu, H. Li, and F. Gao, **Design of Vehicle Remote Monitoring System Based on 4G and FlexRay**, in *2018 IEEE 18th International Conference on Communication Technology (ICCT)*, pp. 478–482, 2018.

[3] E. Calvanese Strinati *et al.*, **6G: The Next Frontier: From Holographic Messaging to Artificial Intelligence Using Subterahertz and Visible Light Communication**, *IEEE Veh. Technol. Mag.*, vol. 14, no. 3, pp. 42–58, 2019.

[4] R. P. Hudhajanto, I. G. P. Astawa, and A. Sudarsono, **Covert communication in mimo-ofdm system using pseudo random location of fake subcarriers**, *Emit. Int. J. Eng. Technol.*, vol. 4, no. 1, pp. 150–163, 2016.

[5] S. Kaur, L. Kansal, G. S. Gaba, and N. Safarov, **Survey of Filter Bank Multicarrier (FBMC) as an efficient waveform for 5G**, *Int. J. Pure Appl. Maathematics*, vol. 118, no. 7, pp. 45–49, 2018, [Online]. Available: http://www.ijpam.eu.

[6] Z. Zhang, H. Wang, G. Yu, Y. Zhang, and X. Wang, **Universal filtered multi-carrier transmission with adaptive active interference cancellation**, *IEEE Trans. Commun.*, vol. 65, no. 6, pp. 2554–2567, 2017.

[7] F. T. Monteiro *et al.*, **Experimental evaluation of pulse shaping based 5G multicarrier modulation formats in visible light communication systems**, *Opt. Commun.*, vol. 457, p. 124693, 2020.

[8] Z. S. Hammed, S. Y. Ameen, and S. R. M. Zeebaree, **Massive MIMO-OFDM performance enhancement on 5G**, in *2021 29th International Conference on Software, Telecommunications and Computer Networks, SoftCOM 2021*, pp. 1–6, 2021.

[9] P. C. Chen and B. Su, **Filter optimization of out-of-band radiation**

with performance constraints for GFDM systems, in *IEEE Workshop on Signal Processing Advances in Wireless Communications, SPAWC*, 2017, vol. 2017, pp. 1–5, Jul 2017.

[10] T. Kebede, Y. Wondie, J. Steinbrunn, H. B. Kassa, and K. T. Kornegay, **Multi-carrier waveforms and multiple access strategies in wireless networks: Performance, applications, and challenges**, *IEEE Access*, vol. 10, pp. 21120–21140, 2022.

[11] M. Rico-Martinez, C. C. C. Vasquez, S. I. Rodriguez, G. M. V. Duran, and I. T. Monroy, **Comparison of performance between OFDM and GFDM in a 3.5 GHz band 5G hybrid Fiber-Wireless link using SDR**, in *2018 International Topical Meeting on Microwave Photonics (MWP)*, pp. 1–4, 2018.

[12] C. Sharma, S. K. Tomar, and A. Kumar, **A comparison of GFDM and OFDM at same and different spectral efficiency condition**, in *Intelligent Communication Technologies and Virtual Mobile Networks: ICICV 2019*, pp. 282–293, 2020.

[13] R. Gerzaguet *et al.*, **The 5G candidate waveform race: a comparison of complexity and performance**, *Eurasip J. Wirel. Commun. Netw.*, vol. 2017, no. 1, pp. 1–14, 2017.

[14] T. Pitchaiah and R. S. Yarrabothu, **Performance analysis of OQAM based GFDM 5G systems under line of sight fading scenarios**, in *2017 International Conference on Intelligent Sustainable Systems (ICISS)*, pp. 602–606, 2017.

[15] S. Sun, G. R. Maccartney, and T. S. Rappaport, **A novel millimeter-wave channel simulator and applications for 5G wireless communications**, in *IEEE International Conference on Communications*, pp. 1–7, 2017.

[16] A. Al-Omary, **Investigating the visibility of 28 and 73 GHz frequency bands for outdoor MIMO channel**, *Int. J. Comput. Digit. Syst.*, vol. 9, no. 3, pp. 503–513, 2020..

[17] Z. A. Shamsan,**A Statistical Channel Propagation Analysis for 5G mmWave at 73 GHz in Urban Microcell**, *Lect. Notes Data Eng. Commun. Technol.*, vol. 72, pp. 748–756, 2021.

[18] E. D. Wardihani, H. W. Astuti, A. Suharjono, and S. **Pramono, Performance of 5G-NR under Semarang Channel Model**, in *IOP Conference Series: Materials Science and Engineering*, vol. 1096, no. 1, p. 12078, 2021.

[19] Z. S. Hammed, S. Y. Ameen, and S. R. M. Zeebaree, **Investigation of 5G Wireless Communication with Dust and Sand Storms**, *J. Commun.*, vol. 18, no. 1, 2023.

[20] X. Zhang, M. Jia, L. Chen, J. Ma, and J. Qiu, **Filtered-OFDM - Enabler for flexible waveform in the 5th generation cellular networks**, in *2015 IEEE Global Communications Conference, GLOBECOM 2015*, pp. 1–6, 2015.

[21] Z. A. Sim, F. H. Juwono, R. Reine, Z. Zang, and L. Gopal, **Performance of**

GFDM systems using quadratic programming pulse shaping filter design, *IEEE Access*, vol. 8, pp. 37134–37146, 2020.

[22] A. Mohammadian, A. Mohammadi, A. Abdipour, and M. Baghani, **Spectral analysis of GFDM modulated signal under nonlinear behavior of power amplifier**, *Wirel. Networks*, vol. 27, no. 1, pp. 137–149, 2021.

[23] S. Mohanraj and P. Dananjayan, **Performance analysis of GFDM system using LDGT for varying window**, in *2019 IEEE International Conference on System, Computation, Automation and Networking, ICSCAN 2019*, pp. 1–4, 2019.

[24] M. Matthe, N. Michailow, I. Gaspar, and G. Fettweis, **Influence of pulse shaping on bit error rate performance and out of band radiation of Generalized Frequency Division Multiplexing**, in *2014 IEEE International Conference on Communications Workshops, ICC 2014*, pp. 43–48, 2014.

[25] P. Kumar, L. Kansal, G. S. Gaba, M. Mounir, A. Sharma, and P. K. Singh, **Impact of peak to average power ratio reduction techniques on Generalized Frequency Division Multiplexing for 5th generation systems**, *Comput. Electr. Eng.*, vol. 95, p. 107386, 2021.

[26] Z. S. Al-Timime, **Signal Denoising Using Double Density Discrete Wavelet Transform**, *Al-Nahrain J. Sci.*, vol. 20, no. 4, pp. 125–129, 2017.

[27] G. Wunder *et al.*, **5GNOW: Non-orthogonal, asynchronous waveforms for future mobile applications**, *IEEE Commun. Mag.*, vol. 52, no. 2, pp. 97–105, 2014.

[28] Z. A. Shamsan, **Dust Storm and Diffraction Modelling for 5G Spectrum Wireless Fixed Links in Arid Regions**, *IEEE Access*, vol. 7, pp. 162828–162840, 2019.

[29] E. M. Alfaroby, N. M. Adriansyah, and K. Anwar, **Study on channel model for Indonesia 5G networks**, in *2018 International Conference on Signals and Systems (ICSigSys)*, pp. 125–130, 2018.

[30] G. R. MacCartney and T. S. Rappaport, **Rural macrocell path loss models for millimeter wave wireless communications**, *IEEE J. Sel. areas Commun.*, vol. 35, no. 7, pp. 1663–1677, 2017.

[31] M. K. Elmezughi and T. J. Afullo, **An Efficient Approach of Improving Path Loss Models for Future Mobile Networks in Enclosed Indoor Environments**, *IEEE Access*, vol. 9, pp. 110332–110345, 2021.

[32] C.-X. Wang, J. Bian, J. Sun, W. Zhang, and M. Zhang, **A survey of 5G channel measurements and models**, *IEEE Commun. Surv. Tutorials*, vol. 20, no. 4, pp. 3142–3168, 2018.

[33] E. M. M. Abuhdima *et al.*, **The effect of Dust and Sand on the 5G Millimeter-Wave links**, 2021 IEEE Int. Conf. Wirel. Sp. Extrem. Environ. WiSEE 2021, pp. 60–65, 2021.

[34] N. Ram, H. Gao, H. Qin, M. T. Oo, and Y. T. Htun, **Statistical Channel Modelling of Millimetre Waves at 28 GHz and 73 GHz Frequency**

Signals Using MIMO Antennas, in *Journal of Physics: Conference Series*, 2021, vol. 1732, no. 1, pp. 12184.

[35] A. Kumar, A. Kumar, and A. Kumar, **A broadband circularly polarized monopole antenna for millimeter-wave short range 5G wireless communication**, *Int. J. RF Microw. Comput. Eng.*, vol. 31, no. 2, pp. e22518, 2021.

[36] Z. Xiao *et al.*, **A survey on millimeter-wave beamforming enabled UAV communications and networking**, *IEEE Commun. Surv. Tutorials*, vol. 24, no. 1, pp. 557–610, 2021.

[37] A. Xia *et al.*, **28 GHz MIMO channel capacity analysis for 5G wireless communication systems**, in *2018 12th International Symposium on Antennas, Propagation and EM Theory (ISAPE)*, pp. 1–4, 2018.

[38] J. Vihriälä *et al.*, **Numerology and frame structure for 5G radio access**, in *2016 IEEE 27th annual international symposium on personal, indoor, and mobile radio communications (PIMRC)*, pp. 1–5, 2016.

[39] M. Mukhlisin, H. W. Astuti, and E. D. Wardihani, **Rain Rate Influence on Performance of Semarang 5G-NR Channel Model**, in *International Conference on Innovation in Science and Technology (ICIST 2020)*, pp. 110–113, 2021.

[40] A. Hilario-Tacuri and A. Tamo, **BER performance of mm-Wave based systems in rainfall scenarios**, in *2018 IEEE XXV International Conference on Electronics, Electrical Engineering and Computing (INTERCON)*, pp. 1–4, 2018.

[41] A. E. Jayati, Wirawan, T. Suryani, and Endroyono, **Nonlinear Distortion Cancellation using Predistorter in MIMO-GFDM Systems,** *Electronics*, vol. 8, no. 6, p. 620, 2019.

[42] E. Çatak and L. Durak-Ata, **Waveform design considerations for 5G wireless networks**, *Towar. 5G Wirel. Networks-A Phys. Layer Perspect.*, pp. 27–48, 2016.